EXPERIMENTAL AND THEORETICAL STUDY OF VOCAL FOLD REPLICAS ELASTICITY WITHOUT AND WITH INCLUSIONS

Mohammad Ahmad, Anne Bouvet, Xavier Pelorson, Annemie van Hirtum

27th INTERNATIONAL CONGRESS ON SOUND AND VIBRATION
12 – 16 July 2020, Prague

ICSV27 PRAGUE

Annual Congress of the International Institute of Acoustics and Vibration (IIAV)

EXPERIMENTAL AND THEORETICAL STUDY OF VOCAL FOLD REPLICAS ELASTICITY WITHOUT AND WITH INCLUSIONS

Mohammad Ahmad, Anne Bouvet, Xavier Pelorson and Annemie Van Hirtum
LEGI, UMR CNRS 5519, Grenoble Alpes University, France
e-mail: mohammad.ahmad@univ-grenoble-alpes.fr, annemie.vanhirtum@univ-grenoble-alpes.fr

The vocal fold vibration, and hence acoustic source properties of voiced speech sounds, rely on the vocal folds elasticity which is therefore a crucial part of the underlying fluid-structure interaction for healthy as well as pathological conditions. The human vocal folds are an extremely complex structure. Therefore, physical studies often rely on simplified mechanical vocal folds replicas. Two types of replicas proposed in literature are considered, i.e. multi-layer silicone replicas and a pressurized latex replica. For both replica types, the mechanical properties are experimentally characterized by measuring their Young's modulus and frequency response. Next, a simple physical model is proposed and validated in order to predict the effective Young's modulus of silicone replicas from their individual constituents. This allows to account for their multi-layer composition characterising normal human vocal folds with different degree of detail. In the future, inclusions in the replica mimicking structural vocal fold pathologies for instance associated with polyps, scars, etc. can be accounted for.

Keywords: Vibration, Phonation, Vocal folds replicas, Structural mechanics

1. Introduction

The acoustic and aerodynamic properties of voice depends on the structural properties of the vocal folds (VFs). Systematically studying the influence of varying structural properties of the human VFs on voice quality is not feasible without invasive muscular stimulation. Therefore, deformable mechanical VFs replicas side by side with theoretical models can be used in systematic studies. Several VFs pathologies can alter the material properties of the vibratory tissue, e.g., the presence of an inclusion or a scar. In this work, it is aimed to characterize the structural properties of deformable mechanical VFs replicas introduced in Section 2 in order to be able to further systematically investigate and quantify the effect of structural VFs pathologies like inclusions. A theoretical model that predicts the effect of the presence of multiple layers, and eventually inclusions, on the VFs elasticity is compared with experimental results.

2. Deformable mechanical VF replicas and molded silicone specimen

Two types of 1:1 scaled deformable mechanical VF replicas are considered: pressurised latex tube (PLT) replica and silicone (M5, MRI and EPI) replicas as shown in Fig. 1. The PLT replica consists of

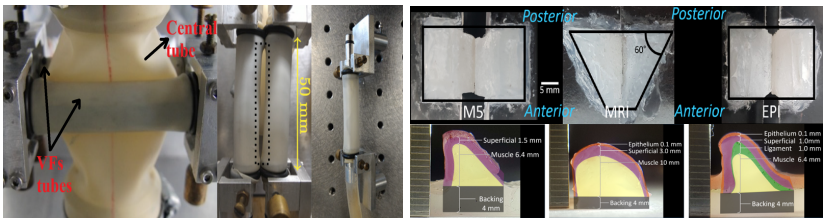

(a) PLT replica (b) silicone molded replicas

Figure 1: Deformable mechanical VF replicas: a) PLT, b) silicone (M5, MRI, EPI) [1].

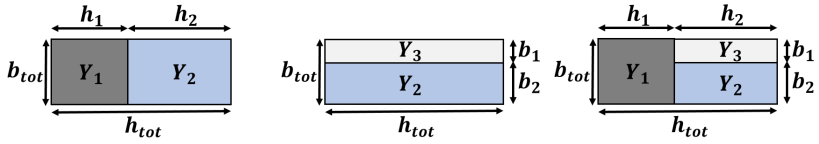

(a) 2L - horizontal (b) 2L - vertical (c) 3L - combined

Figure 2: Stacked silicone bone-shaped specimens ($h_{tot} = 80$ mm and $b_{tot} = 10$ mm).

two latex tubes (0.2 mm thick, length $l_{PLT} = 50$ mm, and diameter $d_0 = 11$ mm). The latex tube covers a hollow rigid support and is filled with distilled water supplied by a water column whose height can be controlled to set the internal water pressure P_{PLT}, thus mimicking the elasticity adjusting function of a human VF. In this study, P_{PLT} range was increased and decreased between 500 Pa and 6500 Pa with a step of 500 Pa (or 100 Pa for image analysis in Section 3.3). Silicone replicas consist of an overlay of molded silicone layers that approximate the multi-layer (ML) structure of a human VF [2, 1]. The elasticity Young modulus of each layer (up to 57.5 kPa) fits within elasticity values (up to 60 kPa) reported for the human VF structure (up to 60 kPa). The influence of their ML composition (constituents Young's modulus Y) on their overall elasticity, i.e. effective Young's modulus Y_{eff}, is studied experimentally using molded ML bone-shaped specimens of working length $h_{tot} = 80$ mm, thickness $b_{tot} = 10$ mm and width 15 mm (and hence initial cross section area $S_0 = 150$ mm^2) as depicted in Fig. 2. Specimens composed of one (1L), two (2L) and three (3L) stacked layers are considered. Layer dimensions and stacking orientations, vertical (b) or horizontal (h) with respect to the longitudinal specimen axis z, are varied. Three different silicone mixture constituents – c_1 with $Y_1 \approx 52.0$ kPa, c_2 with $Y_2 \approx 10.4$ kPa and c_3 with $Y_3 \approx 4.9$ kPa [1] – are used to obtain 14 specimens summarised in Table 1: 3 with (1L), 6 with 2L and 5 with 3L. Geometrical layer ($1 \leq i \leq 3$) ratios are obtained by normalising its dimension (h_i or b_i) by the corresponding specimen dimension (h_{tot} or b_{tot}), *i.e.* $H_{i(hor)} = h_i/h_{tot}$ for horizontal and $H_{i(ver)} = b_i/b_{tot}$ for vertical stacking. Thus, 2L specimens are characterised by H_1 and 3L specimens by H_1 and H_2 normalised with respect to the orientation of layer $i+1$, *i.e.* layers 2 and 3 respectively.

3. Experimental methods for mechanical characterisation: Y_{eff} and FRF

3.1 Using mechanical press: Y_{eff} of silicone specimens

An electro-mechanical press (3369, Instron Corp.) with 50 kN force sensor (2530-445/71212, Instron Corp., accuracy 0.2%), shown in Fig. 3(a), is used for uni-axial tension testing of silicone specimen along the longitudinal z-axis with typical charges are up to 8 N. The press was set for displacement control imposing four maximum elongations Δl (25, 50, 100, and 150 mm). The deformation rate was

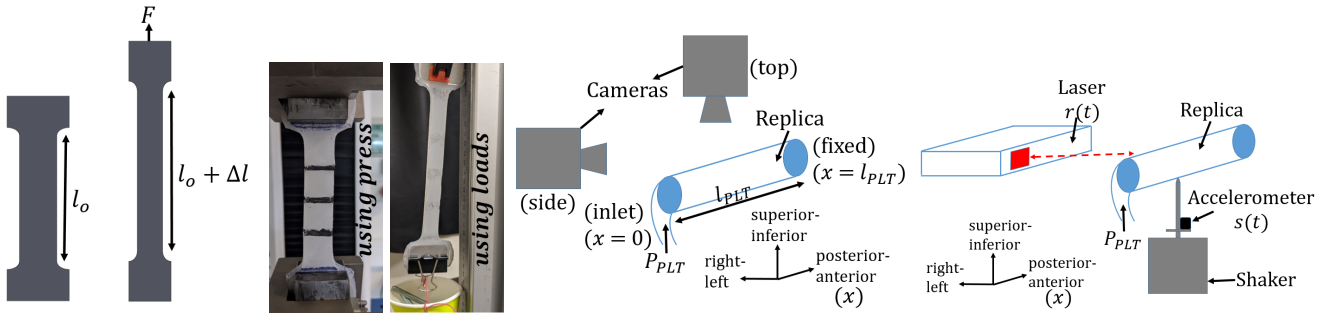

(a) tensile test on silicone specimen (b) VF imaging $f(P_{PLT})$ (c) FRF $f(P_{PLT})$

Figure 3: Experimental methods: a) Y_{eff} of specimen, b) Y_{eff} of PLT replica, c) FRF of PLT replica.

set to 1 mm/s for the 25, 50 and 100 mm elongations and to 2 mm/s for 150 mm elongation. Force and elongation time series (sampling rate of 10 Hz) were measured during loading of the specimens. No plastic deformation was observed following their unloading (5 mm/s). Due to the relative softness of the tested silicone specimens ($F \leq 8$ N compared to a 50 kN force sensor range), a moving-average filter with variable window size was used to smooth the force sensor data. Fig. 4(a) shows a typical measured and smoothed force-elongation curve for a horizontally stacked 2L molded specimen (9 in Table 1). Furthermore, the initial specimen length $l_0 \gtrapprox h_{tot}$ (design value), layers heights $l_i \geq h_i$ (design values) and cross section areas $\mathcal{S} \leq S_0$ are measured using a 0.01 mm-precision caliper (Mitutoyo 500-196-30). For horizontally stacked layers, $\mathcal{S}_i$ and l_i are measured for each layer i after loading the specimen to each elongation. The averaged cross-section area of the specimen is obtained as a weighted mean using the layers' heights l_i and their sum for normalization. A quadratic fit to the weighted averaged areas of each elongation is then obtained (coefficient of determination $R^2 > 0.9$) as shown in Fig. 4(b). Stress σ and strain ϵ are then calculated as $\sigma = F/\mathcal{S}$ and $\epsilon = \Delta l/l_0$. Young's modulus Y_{eff} is then estimated for each specimen by fitting the quasi-linear part of the stress-strain curves as shown in Fig. 4(c). Fig. 4(d) shows the estimated values for three specimens (1L, 2L and 3L labelled 2, 9 and 13 in Table 1) for four different maximum elongations Δl. For each specimen, plotted values show little discrepancy (standard deviation 8% (1L), 7% (2L) and 11% (3L)) so that the reported Y_{eff} hereafter corresponds to the mean value for four maximum elongations.

3.2 Using precision loading: Y_{eff} of silicone specimens

Uni-axial tension testing of silicone specimen is also performed by fixing one end and adding precision weights in increments as shown in Fig. 3(a). The added weight m is measured with a 0.01 g-precision scale (Vastar 500G X 0 01G). Added increments range between 5 and 20 g, while total added weights

	Label		Label	Stacking	H_1	Layers		Label	Stacking	H_1	H_2	Layers
1-layer	1 (c_1)	**2-layer**	4	Ver	0.20	c_2/c_3	**3-layer**	10	Ver Ver	0.25	0.50	$c_2/c_3/c_2$
	2 (c_2)		5	Ver	0.50	c_2/c_3		11	Ver Ver	0.25	0.50	$c_1/c_2/c_1$
	3 (c_3)		6	Ver	0.50	c_1/c_2		12	Ver Ver	0.25	0.40	$c_1/c_2/c_3$
			7	Hor	0.20	c_2/c_3		13	Hor Hor	0.20	0.40	$c_1/c_2/c_3$
			8	Hor	0.50	c_2/c_3		14	Hor Ver	0.20	0.50	$c_1/c_2/c_3$
			9	Hor	0.50	c_1/c_2						

Table 1: Molded silicone specimen: 1-layer (1 to 3), 2-layer (4 to 9) and 3-layer (10 to 14).

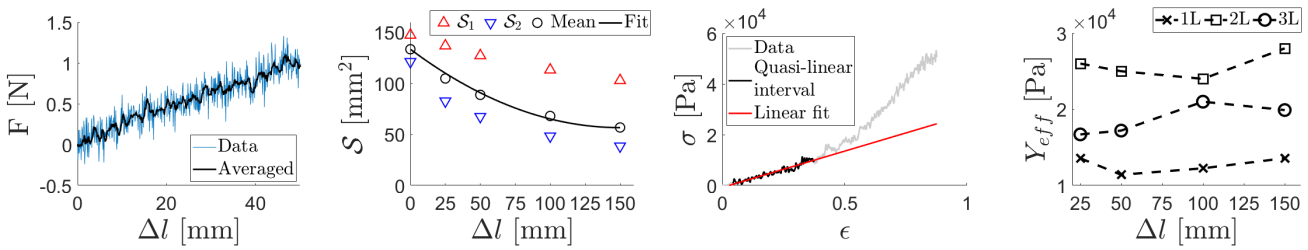

Figure 4: Example of mechanical press data analysis and fits ($R^2 > 0.9$) for 2L specimen (9 in Table 1): a) force-elongation data smoothing (0.7 mm window), b) cross-section area fit $S(\Delta l)$, c) stress-strain curve ($\Delta l \leq 150$ mm) and linear fit ($\epsilon < 38\%$, $\Delta l = 44$ mm), d) mean Y_{eff}, standard deviation $\approx 10\%$.

amount up to 416 g. The initial specimen length $l_0 \gtrapprox h_{tot}$ (design value), layer height $l_i \geq h_i$ (design value) and elongation Δl are measured (1 mm precision ruler) after each weight addition, whereas cross section areas $\mathcal{S} \leq S_0$ are measured (0.01 mm precision caliper) less frequently (every Δl increment of 17 mm). Measured elongations Δl yield up to 255 mm. Forces F resulting from the added masses ($F = m \cdot g$ with $g = 9.81$ m/s^2) are linearly fitted as a function of measured elongation ($R^2 > 0.9$) to produce a force-elongation curve as illustrated in Fig. 5(a). A quadratic fit ($R^2 > 0.9$) is applied to the weighted mean of the measured cross-section areas as shown in Fig. 5(b). For each specimen, the quasi-linear part of the stress-strain curve is fitted to estimate Y_{eff} (Fig. 5(c)). This method is particularly useful for soft specimens for which force data gathered using the mechanical press are very noisy.

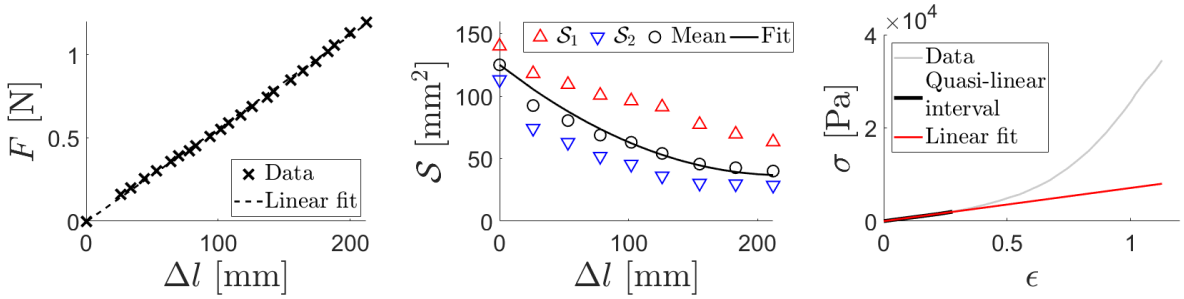

Figure 5: Example of precision loading data analysis and fits ($R^2 > 0.9$) for 2L specimen (8 in Table 1): a) force-elongation data fit, b) cross-section area fit $S(\Delta l)$, c) stress-strain curve ($\Delta l \leq 200$ mm) and linear fit ($\epsilon < 30\%$, $\Delta l = 54$ mm).

3.3 Using image analysis: Y_{eff} of PLT replica

Increasing internal water pressure P_{PLT} in the PLT replica expands the latex tubes and hence their local diameter $d \geq d_0$. As the replica can be considered as an inhomogeneous material, i.e., consists of both latex and water, the relationship between the increasing pressure and the replica's deformation, characterized by the replica's diameter d, is not governed by the Young's modulus of the latex, but by an effective Young's modulus Y_{eff}. At first, P_{PLT} is set to 500 Pa and the associated diameter is chosen to be the reference diameter, denoted d_{ref}. The internal water pressure is then increased by 100 Pa increments. For each P_{PLT} value top view (transverse plane, Motion BLITZ Eosens Cube 7, 726 μs

shutter, 11 aperture) and side view (sagittal plane, Nikon D3100, with AF-S NIKKOR 18-70 mm lens, 2 ms shutter, 4.3 aperture) images are taken (see Fig. 3(b)). For each viewing plane, the replica's edges are detected as illustrated in Fig. 6(a) from which diameter $\hat{d}$ along the posterior-anterior axis x is assessed for increasing and decreasing P_{PLT}. From these edges, mean diameter values $\overline{d}$ and standard deviations $\leq 4\%$ (Fig. 6(b)) as well as a maximum bending diameter d_{ben} (squares in Fig. 6(a)) are extracted for each P_{PLT}. Strain ϵ is obtained as $\epsilon = (\hat{d} - d_{ref})/\hat{d}$ for $\hat{d} = \overline{d}$, $\hat{d} = d_{ben}$ or yet $\hat{d} = d(x)$ estimated in a small region of 4 mm around $x = 0.4 \cdot l_{PLT}$, $x = 0.5 \cdot l_{PLT}$ and $x = 0.6 \cdot l_{PLT}$. Fig. 6(c) shows a resulting pressure-deformation curve form which Y_{eff} is estimated (slope of a linear data fit ($R^2 > 0.9$)).

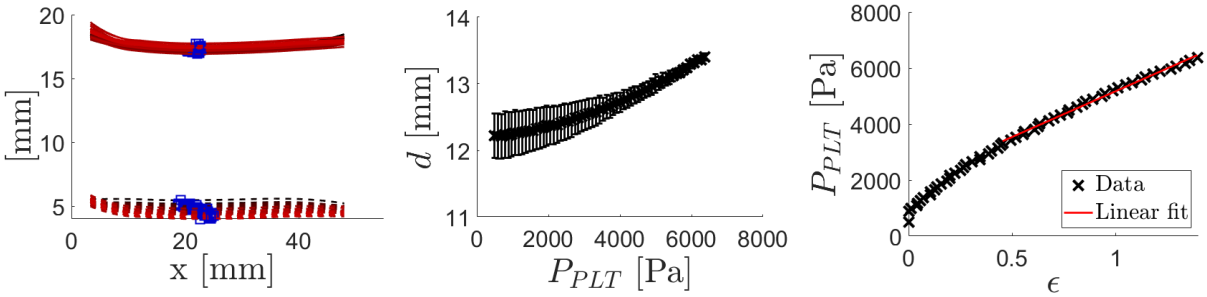

(a) edges and maximum bending (b) $\overline{d}$ and std (c)

Figure 6: PLT replica imaging: a) detected upper (solid line) and lower (dashed line) edges in the saggital plane (side view) and position of maximum bending (square), b) mean diameter $\overline{d}(x)$ and std (bars), c) stress-strain curve and fit to quasi-linear portion ($R^2 > 0.9$).

3.4 Frequency response function: mechanical resonances of PLT replica

To estimate the mechanical resonance frequencies f_j, the frequency response function (FRF) is measured as a function of P_{PLT}. Two points p_1 and p_2 along the posterior-anterior length of the PLT replica l_{PLT} are used for both force excitation and deformation response recording as illustrated in Fig. 3(c). The points are located at $x = 0.4 \cdot l_{PLT}$ and $x = 0.6 \cdot l_{PLT}$, respectively. An 11 s linear sweep signal with a frequency range from 60 up to 250 Hz is used to excite the replica using a shaker (Modal Shop, K-2007E01) equipped with an excitation rod (length 82.5 mm and diameter 3.7 mm). A piezoelectric accelerometer (PCB ICP, 353B18) is used to capture the excitation signal. The response is recorded using a laser transceiver (Panasonic HLG112AC5, 655 nm wavelength, accuracy 80 µm). Excitation signal $s(t)$ and response signal $r(t)$, sampled at 10 kHz, are transformed into the frequency domain ω to calculate the transfer function as $FRF = R(\omega)/S(\omega)$ [3]. Fig. 7(a) shows a typical FRF of the PLT VF replica, exhibiting four resonance peak frequencies f_j ($j = 1 \ldots 4$). As the FRF methodology assumes a linear system [4], the time-invariance (and hence the repeatability of FRF measurements) and reciprocity (and hence that excitation and response positions can be interchanged) of the FRF measurements is confirmed. Fig. 7(b) shows FRF measurements for increasing P_{PLT}.

4. Analytical model to predict Y_{eff}

To predict the effective Young's modulus Y_{eff} of multi-layer silicone specimens from the Young's modulus Y of their individual constituents and their stacking (dimensions and orientation), two analytical models are developed for both horizontal and vertical stacking of layers as illustrated in Fig. 2. The models assume perfectly bounded, parallel and isotropic layers that remain parallel after deformation,

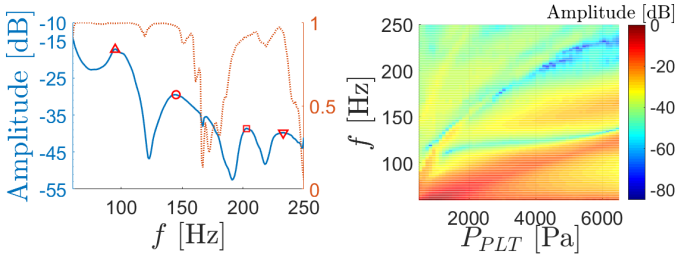

(a) $P_{PLT} = 3700$ Pa (b) $500 \leq P_{PLT} \leq 6500$ Pa

Figure 7: FRF amplitude for PLT replica: a) FRF (solid line) and coherence (dashed line) for $P_{PLT} = 3700$ Pa indicating 4 resonance peaks (symbols), b) FRF overview for $500 \leq P_{PLT} \leq 6500$ Pa.

and represent linear stress-strain behaviour. For horizontal stacking, a height weighted average of Y_i results in $Y_{eff} = \sum_i h_i / \sum_i (h_i/Y_i)$, where i indicates the layer, Y_i is the layer's Young's modulus, and h_i is the layer's dimension (height) along the z (forcing) axis. For vertical stacking, a weighted harmonic mean with respect to b_i results in $Y_{eff} = \sum_i b_i Y_i / \sum_i b_i$, where b_i is the layer dimension (thickness) perpendicular to the z axis. Combining both models allows to estimate Y_{eff} for more complex ML specimens with both horizontally and vertically stacked layers as depicted in Fig. 2(c). It is noted that predicted Y_{eff} do solely depend on the overall layer composition and not on their order or distribution.

5. Results

5.1 Mechanical characterisation of the PLT replica: resonance peaks and Y_{eff}

Mechanical resonances are extracted as a function of internal water pressure P_{PLT} from the measured FRF. At each P_{PLT}, up to four resonance frequencies f_j ($j = 1 \ldots 4$) are detected as plotted in Fig. 8(a). Due to the time-invariance and reciprocity of the FRF measurements the f_j discrepancy between different measurements (interchanging excitation and response position, repeatability) was within 5%. Detected resonance peaks and their properties (such as the bandwidth [3]) need further analysis to estimate the stiffness and damping associated with each resonance.

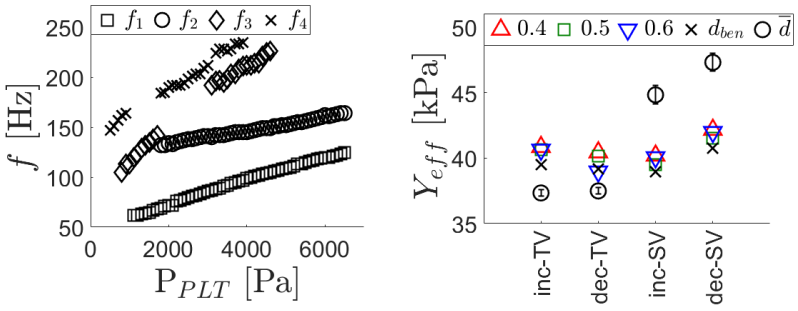

(a) resonances f_j (b) Y_{eff}

Figure 8: PLT replica: a) Example of detected resonance frequencies as a function of increasing P_{PLT}, b) Calculated effective Young's modulus of the replica from four different measurements.

Effective Young's modulus Y_{eff} for the PLT replica are obtained for each of the diameter estimations $\hat{d}$ outlined in Section 3.3: mean diameter $\overline{d}$, diameter at maximal bending d_{ben} and in 4 mm regions ($\Delta x = 0.08 \cdot l_{PLT}$) at positions $x = 0.4 \cdot l_{PLT}$, $x = 0.5 \cdot l_{PLT}$ and $x = 0.6 \cdot l_{PLT}$. Fig. 8(b) shows

resulting estimated Y_{PLT} from imaging for increasing (inc) and decreasing (dec) P_{PLT} for both camera views, *i.e.* top view (TV) and side view (SV). Estimated values $Y_{eff} \approx 40 \pm 5$ kPa are within the range associated with the stiff epithelium layer for a human VF [1]. From Fig. 8(b), applying overall diameter estimation $\hat{d} = \overline{d}$ (circles in Fig. 8(b)) results in either an underestimation (less rigid, top view TV) or overestimation (more rigid, side view SV) Y_{eff} of values obtained for the other more localised (near the center) $\hat{d}$ estimations. This might indicate that the side view, hindered by the rigid support of the latex tube, underestimates deformation and hence overestimates Y_{eff} whereas the top view accounts for 'false' deformation due to the constraints near the fixed boundaries. Following this reasoning, localised diameter estimations result in the most accurate $Y_{eff} = 40.5 \pm 1$ kPa estimation. The discrepancy ($\leq 6\%$) is low between increasing or decreasing P_{PLT} series or between top and side views.

5.2 Measured and predicted Y_{eff} for silicone specimens and silicone replicas

The Young's moduli Y for one-layer (1L) and effective Young's moduli Y_{eff} for two-layer (2L) and three layer (3L) silicone specimens outlined in Table 1 are plotted in Fig. 9. Experimental estimations obtained from tensile test measurements using the mechanical press (Section 3.1, squares) and precision loading (Section 3.2, circles) are shown for all specimen. Model predictions (Section 4, crosses) of Y_{eff} are indicated for the 2L and 3L specimens.

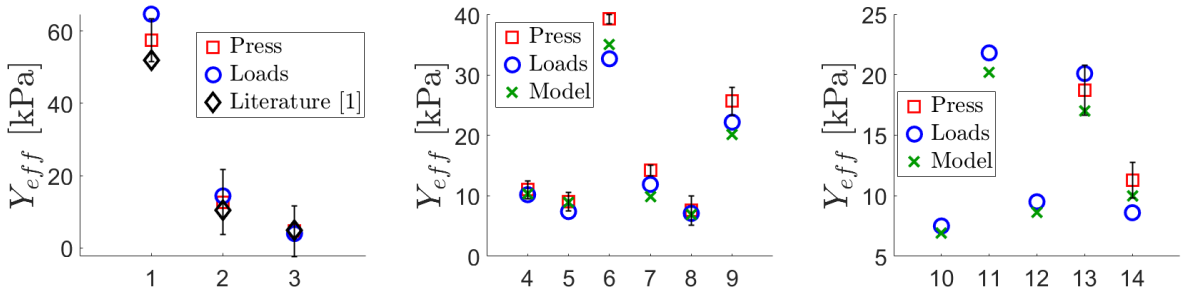

(a) 1L (b) 2L (c) 3L

Figure 9: Effective Young's modulus Y_{eff} of silicone specimens: a) 1L, b) 2L and c) 3L.

Measured Y_{eff} are cross-validated by both tensile test techniques (loading and press) for 2L specimen (4 up to 9) and some 3L specimen (13 and 14) as the averaged discrepancy yields 12% so that either technique result in an accurate estimation of Y_{eff}. The loading technique is used to experimentally determine Y_{eff} for additional 3L specimen (10 up to 12). Furthermore, for horizontally stacked specimen (9 in Table 1) it is verified (discrepancy $\leq 4\%$) that tensile testing is independent of the specimen's orientation by repeating the loading experiment with the specimen flipped upside down.

From Fig. 9(b) (2L specimens) and Fig. 9(c) (3L specimen) is seen that modeled Y_{eff} values using the analytical models presented in section 4 match well with measured values for both horizontally as vertically stacked layers. Indeed, the average error between modeled and measured values yields 11%, which is of the same order of magnitude as the discrepancy between measured values. The same accuracy holds for 3L specimen 14 (14% error) containing both horizontally and vertically stacked layers. Moreover, it is noted that Y_{eff} obtained for 2L specimens 8 and 9 are similar ($\leq 2\%$ discrepancy) to those obtained for 3L specimens 10 and 11 respectively. This further confirms that the applied model approach can be used to estimate Y_{eff} as this verifies the model property that for similar layer constituents and geometrical

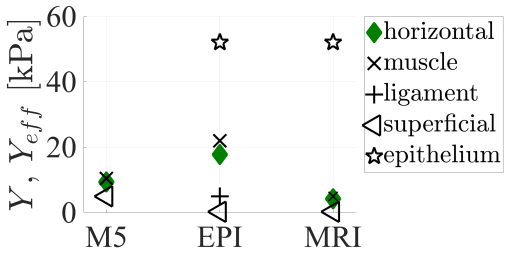

Figure 10: Modeled Y_{eff} (filled diamonds) assuming horizontal layer stacking of ML silicone VF replicas (M5, EPI and MRI) and Y of individual constituents mimicking anatomical layers [1].

ratio Y_{eff} is independent from the layer order or layer distribution.

As a first approximation silicone VF replicas (Fig. 1(b)) can be considered as horizontally stacked layers. Modelled Y_{eff} based on the Y of the different anatomical layers are plotted in Fig. 10. Values vary significantly between replicas – 9.3 kPa (M5), 17.7 kPa (EPI) and 4.1 kPa (MRI) – and are low compared to the PLT replica ($Y_{eff} \approx 40$ kPa).

6. Conclusion and perspectives

The elasticity of VFs replicas, *i.e.* effective linear Young's modulus and mechanical resonances, are characterized for a deformable pressurized latex replica and multi-layer silicone-molded replicas. For the PLT replica, a value of $Y_{eff} \approx 40$ kPa was found and mechanical resonances were detected to allow in the future to estimate its dynamic properties, i.e., stiffness, damping, and vibrating mass. In the future, it is aimed to relate Y_{eff} to its mechanical features. For silicone moldings, an analytical model of Y_{eff} is validated from tensile test results of 14 stacked (horizontal, vertical or their combination) multi-layer bone-shaped specimens with layer properties pertinent to VF silicone replicas. The model is used to predict Y_{eff} for silicone VF replicas assuming horizontally stacked layers. This preliminary result needs further analysis and it is aimed to relate $Y_{eff} < 20$ kPa to observed vibration properties. It is intended to extent the model validation to pathological structure conditions related to inclusions (cysts, nodules, ..).

Acknowledgements

Funding by Full3DTalkingHead project (ANR-20-CE23-0008-03) and a PhD grant (French Ministry of Education and Research). Prof. G. Combe and F. Girard for electro-mechanical press use and support.

REFERENCES

1. Bouvet, A., Tokuda, I., Pelorson, X. and Van Hirtum, A. Influence of level difference due to vocal folds angular asymmetry on auto-oscillating replicas, *J. Acoust. Soc. Am.*, **147** (2), 1136–1145, (2020).

2. Murray, P. R. and Thomson, S. L. Vibratory responses of synthetic, self-oscillating vocal fold models, *J. Acoust. Soc. Am.*, **132** (5), 3428–3438, (2012).

3. Cisonni, J., Van Hirtum, A., Pelorson, X. and Lucero, J. The influence of geometrical and mechanical input parameters on theoretical models of phonation, *Acta Acust united Ac*, **97** (2), 291–302, (2011).

4. He, J. and Fu, Z.-F., *Modal analysis*, Elsevier (2001).